Investigation of high-speed rubbing behavior of labyrinth-honeycomb seal for turbine engine application[*]

Na ZHANG[1,3], Hai-jun XUAN[†‡1,3], Xiao-jun GUO[2], Chao-peng GUAN[1,3], Wei-rong HONG[1]

(*[1]High-speed Rotating Machinery Laboratory, College of Energy Engineering, Zhejiang University, Hangzhou 310027, China*)
(*[2]China Aviation Powerplant Research Institute, Zhuzhou 412002, China*)
(*[3]Collaborative Innovation Center for Advanced Aero-engine, Beijing 100083, China*)
[†]E-mail: marine@zju.edu.cn

Abstract: The labyrinth-honeycomb seal has been widely used in gas turbine engines as an abradable gas path seal to protect the rotor from wear and damage in rubbing interaction. It usually works with a stepped labyrinth because the knife-edged tips could produce a special dynamic sealing system, and then the minimum clearance is possible between the rotor and stationary component. To investigate the high-speed rubbing behavior between a Hastelloy-X honeycomb material and a GH4169 double stepped labyrinth, nine rubbing tests were conducted using a high-speed abrasion test rig while the blade tip speed varied from 150 to 450 m/s, and the incursion rate from 120 to 360 μm/s. The abradability of honeycomb made from Hastelloy-X was fully verified by analyzing the visual rubbing observations, rubbing forces, and impact acceleration. It is shown that compression deformation happens to the honeycomb material during the rubbing process with the labyrinth blade except for a simple cutting mechanism, which is mainly affected by the parameter of incursion rate. Thermal ablation and oxidation were the main damage occurring on the labyrinth tip and appeared more obviously at a higher blade tip speed. Rubbing forces and impact acceleration were obtained from a piezoelectric dynamometer and acceleration sensor during the rubbing process. At a blade tip speed of 300 m/s and incursion rate of 360 μm/s, radial and tangential forces show their maximum values of 716 N and 871 N, respectively. The peak value of acceleration presents 341g with the highest blade tip speed of 450 m/s and the highest incursion rate of 360 μm/s. All testing results provide a great deal of effective information on high-speed rubbing behavior for the abradablility evaluation of a honeycomb.

Key words: Labyrinth-honeycomb seal, Aeroengine shrouded turbine blade, Abradability, Rubbing mechanism, Rubbing interaction

http://dx.doi.org/10.1631/jzus.A1600367   **CLC number:** TG115.5; V250

1 Introduction

For decades, increasing engine effectiveness and reducing gas leakage have been the hot topics for technology development of turbo engines and other turbo machines (DeMasi-Marcin and Gupta, 1994; Ghasripoor *et al.*, 1997; Fu *et al.*, 2015). Turbo-engine designers seek new solutions to improve engine efficiency. Research shows that a highly effective method is to control the airflow leakage by reducing the radial clearance between the rotary parts and the stationary casing (Dalzell *et al.*, 2002; Dorfman *et al.*, 2002). Ideally zero blade tip clearance could avoid any performance losses. However, a larger clearance has to be designed in a conventional seal for many reasons, such as manufacturing tolerances, the creep elongation of the disk and blade, contraction deformation of the casing, and spindle

vibration and deflection (Rathmann *et al.*, 2007). In the sealing system of turbine-engines, a particular type of rotary seal with several teeth on the rotating shaft called a labyrinth seal is used to minimize the leakage which occurs between rotating and stationary components in turbo-machines. Much of the literature has focused on the sealing performance of a labyrinth seal by means of experiments and simulations. Basic flow mechanisms of leakage reduction in labyrinth seals were identified by Vakili *et al.* (2005) through numerical modeling and experiments, which were helpful in facilitating basic physical understanding and improving seal design.

To increase the efficiency of the labyrinth seal, aero-engine manufacturers began to use a honeycomb seal brazed on a casing surface as an abradable material (Draskovich *et al.*, 1998) to minimize the clearance and protect the labyrinth from deformation and wear (Chen *et al.*, 2008; Shen *et al.*, 2011). From system experiments conducted by Collins *et al.* (2008) at different clearances and pressure ratios, it was found that the worn honeycomb demonstrated a significant increase in mass flow, and the location of tooth to groove had a critical influence on mass flow. In another paper (He *et al.*, 2012), conjugate heat transfer and windage heating in the stepped labyrinth with smooth and honeycomb lands were numerically investigated, and found that the presence of honeycomb cells increased the temperature gradient in the labyrinth fin and significantly decreased the temperature gradient in the stator. A honeycomb seal is an advanced seal structure with good abradability performance under conditions of high temperature and differential pressure (Wiebe, 1994; Potter *et al.*, 2009). A honeycomb core is usually made from metal foils which are usually tens of microns thick, and then it is brazed on the skeleton at high temperature to form the outer ring. The thin wall of the honeycomb which is usually 0.05 mm thick makes it a soft seal material to protect the labyrinth tips (Wu, 2011). When the labyrinth tips run at a high rotating speed, it is easy for a sharp-edged labyrinth to cut out some grooves on the soft cores of the honeycomb seal rings which are mounted on the stationary part, and thus the labyrinth tips are protected from damage and a smaller initial clearance is possible. On the contrary, when the rotary part without labyrinth tips contacts the cores, or when the rotating speed is low, honeycomb cores will be

flattened to form a small clearance. A honeycomb seal is helpful to provide damping to inhibit fluid vibration and improve rotor stability (Wei *et al.*, 2005). In general, a honeycomb is made from nickel-base superalloy with high strength and high-performance, which makes it possible to work under the 900 °C condition for a long life with excellent reliability (Miao, 2008). Composite applications of honeycomb structures and labyrinth seals make even zero-clearance installation possible.

During operation, induced rotor-stator displacements might create an undesirable rubbing interaction between the labyrinth tips and the turbo-engine housing (Schmid *et al.*, 2000), which is coated with a sacrificial abradable material layer, comprised of an abradable coating, metal honeycomb, and silicon rubber (Chupp *et al.*, 2002; Dowson *et al.*, 2004), and this high-speed rubbing behavior is similar to the grinding manufacturing process (Zhang *et al.*, 2015). Then to optimize the material selection and structural design of the metal honeycomb and labyrinth blade, an understanding of their tribological behavior is required. At present, Pratt & Whitney of America (Bill and Shiembob, 1977), Sulzer Innotec of Switzerland (Bardi *et al.*, 2008), University of Sheffield (Stringer and Marshall, 2012), Alstom, the National Research Council Canada (Dadouche *et al.*, 2008), Ohio State University (Padova *et al.*, 2006), *et al.* have developed their own abradable test equipment for abrasion interaction investigation and abradability performance evaluation of abradable seal materials. The most distinguishing characteristic of the new abradable test equipment is that it is able to simulate the high-speed and high-temperature working conditions which are similar to those of actual engines and other turbine or compressor machines. Then more accurate test results can be acquired from abrasion tests. Pychynski *et al.* (2015) studied the rubbing behavior of a single seal fin and a single metal foil, and measured contact forces, friction temperatures, and wear. Bill and Shiembob (1981) evaluated rub tolerance and abradability of two different honeycomb materials by experiments performed in a dynamic abradability rig, and used the volume wear ratio (VWR) to act as a parameter for rub performance of the seal materials. The rub interaction between an abradable material and a nickel alloy

labyrinth seal under different turbo-engine operating conditions was simulated by Delebarre *et al.* (2014) on a new high-speed test rig, and results showed a material deformation wear mechanism at a higher rotation speed, and a material removal wear mechanism at a lower rotation speed. Through interaction force measurement, they found that at low incursion speeds, the increase of the rotation speed induced a gradual increase of the maximum forces, and it was reversed for high incursion speeds. In another paper (Sporer *et al.*, 2004), the performance of a number of metallic honeycombs in gas turbine seal applications was reviewed, including physical and mechanical properties, hot gas corrosion resistance, abradability, and erosion resistance, and results showed that alloy MI2100 offers a potentially superior combination of technical performance and cost advantage for seal honeycomb applications.

As labyrinth seals are widely used in varying applications and configurations, including steam and gas turbines plus compressors, a generic investigation that gives broad insight into worn abradable honeycomb labyrinth seal behavior is required. The results can then be applied to each specific situation as required. However, most current research focuses mainly on the abradable performance evaluation and wear mechanism investigation of abradable coatings (Bounazef *et al.*, 2004; Chupp *et al.*, 2004; Ma and Matthews, 2007; Fois *et al.*, 2013), and the friction and wear properties investigation of rubber (Shen *et al.*, 2015), and experimental data on rubbing interaction between honeycomb structure and labyrinth seal is in short supply. Thus, there is a requirement to produce more conclusive information on worn labyrinths, especially the effects of tooth location and wear profile.

This paper aims to simulate the high-speed rubbing behavior between a Hastelloy-X honeycomb and a GH4169 labyrinth in an aero-engine turbine using an abradable tester and evaluate the wear mechanisms of metal honeycomb material and blade labyrinth. The next section presents detailed information on the test equipment, specimens, and scheme. Then test results are analyzed based on visual rubbing observations, rubbing forces, and impact acceleration. Finally, the results from these studies are summarized.

2 Materials and methods

2.1 Test equipment

High-speed rubbing tests between the shrouded blade labyrinth and the honeycomb seal were conducted on a self-developed abradable tester as shown in Fig. 1 in the High-speed Rotating Machinery Laboratory of Zhejiang University, China. The shrouded blade with labyrinth tips was mounted on a rotating disk with high-strength bolts, and a dummy blade, shorter than the sample one, was fixed at 180° around the disk from the shrouded blade to balance its centrifugal force. The maximum rotating speed of this tester is 16000 r/min, which is in line with the high-pressure rotor speed of aero-engines. The labyrinth tip diameter is 621 mm to obtain the maximum blade tip velocity of 520 m/s which is composed of a 500 mm outside diameter of the simulated metal disk installed with overhang on the flexible shaft and a 60.5 mm effective length of the shrouded blade. The honeycomb sample was mounted through a special clamping fixture on a feeding platform with high precision driven by a servo motor and a reducer to simulate the radial incursion movement of the rotating blade in actual engines, and the allowed incursion rate of the honeycomb sample is between 5 and 1000 μm/s with a control precision of 3 μm/s. A three-component piezoelectric dynamometer with the measurement range of 5000 N and an acceleration sensor of 500g are used to measure the rubbing forces and dynamic impact response between labyrinth tips and honeycomb samples, and a single-lens reflex (SLR) camera is equipped to record the high-speed rubbing process.

2.2 Test materials

A simulated shroud blade is illustrated in Fig. 2, and it was designed with a convenient structure for machining and installation. The twisted blade structure was replaced by a straight blade, and the complex tenon attachment was replaced by a bolt connection. However, the labyrinth structure of the blade tip was the same as that in the aero-engine. The simulated blade has two stepped labyrinths with different tip lengths, which were called the first and the second labyrinth tips. The first and second labyrinth tips are 621 mm and 614 mm long in diameter, respectively. The thickness of the labyrinth tip is 0.6 mm, and the

width is 19.76 mm. The shroud blade and dummy blade were fabricated from GH4169 (Inconel 718, in American standard), a typical super alloy widely used in aero-engines (Ma *et al.*, 2010).

The testing honeycomb is the Hastelloy-X hexagonal cell made from 0.05 mm thick sheet, and the regular hexagonal cell size is 0.8 mm, as shown in Fig. 3. The specimen has a length of 85 mm, a width of 17 mm, and a thickness of 6.9 mm with a 3.5 mm step as shown in Fig. 4. The honeycomb belt was brazed on a flat substrate of 4 mm thickness with the material of Inconel 718. The honeycomb sample used in the rubbing test is illustrated in Fig. 5. Fig. 6 shows the relative position between the honeycomb sample and blade labyrinth.
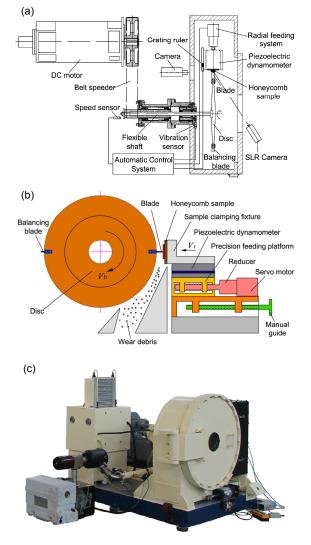

Fig. 1 Structure diagram of abradable tester (a), test schematic diagram (b), and general view of high-speed abradable test rig (c)
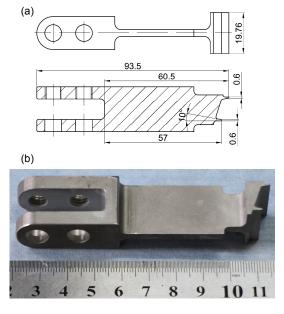

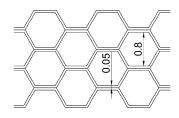Fig. 2 Schematic of simulated blade (a) and its photo (b) (unit: mm)

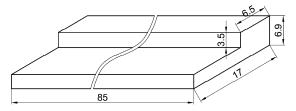Fig. 3 Schematic of the honeycomb structure (unit: mm)

Fig. 4 Geometries of the honeycomb testing sample (unit: mm)

Fig. 5 Honeycomb sample used in rubbing test

2.3 Test scheme

The rubbing behavior between labyrinth tips and honeycomb is influenced by various factors, such as labyrinth tip speed, incursion rate, honeycomb structure size, material, and temperature. In this study, a test matrix is designed to study the influences of labyrinth tip speed and incursion rate of the type which may be encountered in the aero-engines, and test parameters are shown in Table 1.

Three blade tip speeds were selected as representatively low, medium, and high interaction velocities in aero-engines and the incursion rate varied between 120–360 μm/s. The overall incursion depth was kept constant at 1000 μm. To simulate the holding stage of rubbing behavior after the blade labyrinth tips cut grooves on honeycomb material, we introduce an additional parameter of holding time in our rubbing tests.

In testing, as the disk driven by a DC motor, the blade tip speed increased until it reached the target value, and then the feeding platform drove the honeycomb sample to contact the blade tip and continued moving with the same incursion rate until the blade tip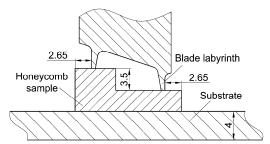 fed into the sample for a depth of 1000 μm. Once the target incursion depth was reached, the feeding platform would hold for 2 s, and then retreated as quickly as possible. Fig. 7 shows the typical incursion process of honeycomb sample during the rubbing test. The incursion depth was recorded by a high-precision grating ruler during the whole process.

2.4 Rubbing forces and acceleration measurements

A Kistler 9257B multi-component dynamometer was selected to measure the radial and tangential rubbing forces, as shown in Fig. 8, and a PCB 352C41 miniature piezoelectric acceleration sensor with a measurement range of ±500g was mounted on the plate to measure the dynamic impact response during the rubbing process. These signals are recorded at a sample frequency of 100 kHz per channel using the high-speed data acquisition system GEN3i with a GN815 data acquisition card.

An integrated circuit piezoelectric (ICP) impulse force test hammer was used to hammer the honeycomb sample on the tapping positions as shown in Fig. 8b. The force calibration was conducted by
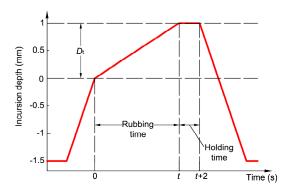
Fig. 6 Location diagram of honeycomb sample and blade labyrinth (unit: mm)

Fig. 7 Typical incursion process during rubbing test

Table 1 Test parameters used in this study

Test No.	Blade tip speed, V_b (m/s)	Incursion rate, V_r (μm/s)	Incursion depth per pass, D_p (μm)	Incursion depth, D_t (μm)	Holding time, T_r (s)
1#	150	120	1.558		
2#	150	240	3.117		
3#	150	360	4.675		
4#	300	120	0.779		
5#	300	240	1.558	1000	2
6#	300	360	2.338		
7#	450	120	0.519		
8#	450	240	1.039		
9#	450	360	1.558		

comparing the force values of the dynamometer and the hammer. A series of test force data in Fig. 9 show little difference with a maximum deviation of 7%, which indicates that it is appropriate for the Kistler dynamometer to measure the rubbing force in tests.
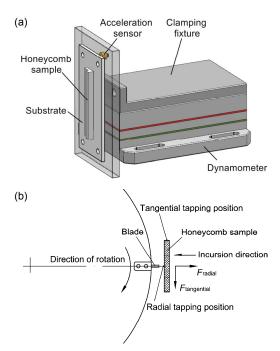

Fig. 8 Experimental device used to measure the rubbing force and impact acceleration (a); Tapping positions of the hammer on the honeycomb sample (b)
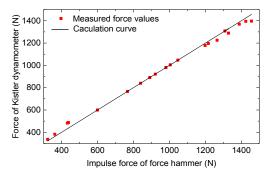

Fig. 9 Calibration curve of Kistler dynamometer signal

3 Test results and discussion

3.1 Analysis of test samples

Turbine blade labyrinth tips impact and rub the metal honeycomb with high velocity, resulting in damage or failure of the honeycomb structure and the wear of the blade labyrinth tip. The impingement and

rubbing action can be demonstrated from the visual observation of the contact pairs after rubbing tests. Two rub-grooves left by turbine blade labyrinth tips on the metal honeycomb and the wear of blade labyrinth tips under all test parameters were observed in Fig. 10. Different worn surface morphologies of metal honeycomb samples and turbine blades present under different parameters. Two rub-grooves were cut out on the material surface with obvious plastic deformation caused by radial extrusion and lateral compression during the rubbing interaction. It seems that the hexagonal porous structure was blocked partly by the plastically deformed material, as shown in Fig. 11, and the lateral compression of the blade labyrinth tip led to the disappearance of peaks and valleys of foils on the edge of the rub-grooves. We also found that a much more serious deformation and larger area of blocked holes are shown on the sample surface with a larger incursion rate than that with a smaller incursion rate, suggesting that incursion rate is one important parameter that affects the ductile deformation of honeycomb material.

During the rubbing process, the contact area between the labyrinth tip and honeycomb sample increases nonlinearly with the rubbing time. The total scraping area S is composed of the scraping areas of the first and the second labyrinth tips S_i (i=1, 2), and the scraping area S_i can be described as the summation of three contact areas, S_{1i}, S_{2i}, and S_{3i}, as shown in Fig. 12.

The bottom contact area is described as

$$S_{1i}(t) = 2R_iT \times \arccos(1-V_rt/R_i), \tag{1}$$

where R_i is the turning radius of the labyrinth tip, T represents the labyrinth tip thickness, V_r is the incursion rate of the honeycomb sample, and t is the rubbing time.

The contact area of the right straight side is described as

$$S_{2i}(t) = R_i^2 \times \arccos\left(1-V_rt/R_i\right) \\ -(R_i-V_rt) \times \sqrt{2V_rt(R_i-V_rt)}. \tag{2}$$

The contact area of the left hypotenuse is described as

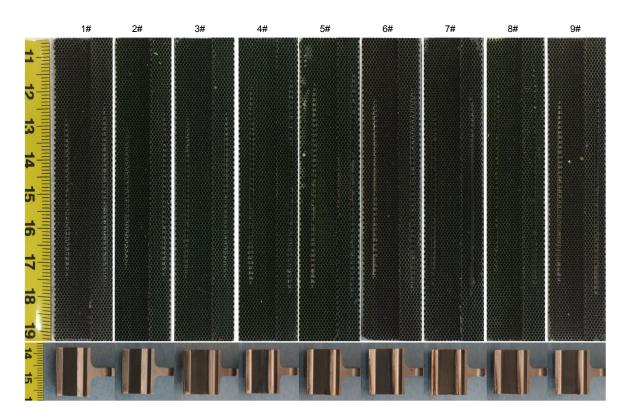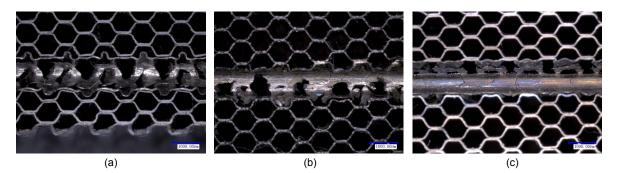**Fig. 10 Honeycomb samples and blade tips after testing**

(a)   (b)   (c)

Fig. 11 Details of blocked honeycomb
(a) Test 1#; (b) Test 6#; (c) Test 7#

Fig. 12 Section view of the contact geometry during rubbing interaction

$$
\begin{aligned}
S_{3i}(t) &= S_{2i}(t)/\cos\alpha \\
&= \Big[R_i^2 \times \arccos(1 - V_\mathrm{r}t/R_i) \\
&\quad - (R_i - V_\mathrm{r}t) \times \sqrt{2V_\mathrm{r}t(R_i - V_\mathrm{r}t)} \Big]\Big/\cos\alpha,
\end{aligned}
$$
(3)

where α is the angle between the hypotenuse and the straight side of the labyrinth tip, and $\alpha = 10°$ in our test.

The total scraping area is given by

$$S(t) = \sum_{i=1}^{2}\left(S_{1i} + S_{2i} + S_{3i}\right)$$

$$= \sum_{i=1}^{2}\left[R_i(2R_i + T + R_i/\cos\alpha) \times \arccos(1 - V_r t/R_i) \right.$$

$$\left. - (1 + 1/\cos\alpha)(R_i - V_r t) \times \sqrt{2V_r t(R_i - V_r t)} \right]. \tag{4}$$

When the blade labyrinth sweeps from the sample surface, a great quantity of frictional heat is generated. Fig. 13 shows the images taken from the video recording of one rubbing test at different times. The effect of frictional heat with an obvious friction spark is clearly shown, which appears primarily at the end of grooves, and the friction spark evident appears gradually as the rubbing time increases. At the beginning of the contact-rubbing, the frictional heat is negligibly small because of the small scraping area between blade tip and flat specimen. With the increase of incursion depth, the rubbing time in a single rubbing cycle prolongs and the scraping area gradually expands, resulting in the increase and congregation of frictional heat. This is consistent with the fact that the spark is generated and brightens gradually with the passage of rubbing time in the video. When the incursion movement is finished and the blade remains for 2 s in the rub-grooves, the friction spark gradually darkens and the build-up of frictional heat is released.

During rubbing tests, the red hot zone with the spark is also associated with blade tip speed. As shown in Fig. 14, the hot zone area increases and the friction spark appears more obvious with the rise of blade labyrinth tip speed, which implies that frictional heat is mainly controlled by blade tip speed.

Because of the frictional heat concentration, thermal ablation and oxidation will occur on the labyrinth tips and metal honeycomb, shown by the sample and blade surface being black and golden. The oxidation of the honeycomb sample occurs first at the end of grooves because of the gathering energy, and then the oxidized area expands as the rubbing action continues until it covers the entire groove. The ablated and oxidized zone of the blade tip is mainly concentrated in the end position, and the thermal ablation and oxidation phenomenon is more obvious at a higher blade tip speed (tests 7#, 8#, and 9#). Moreover, blade tip pictures in Fig. 10 show that the ablated and oxidized area of the blade tip increases with the decrease of incursion rate because of the greater rubbing time between blade tip and honeycomb material action. In the process of thermal ablation, another wear mechanism called smearing occurs on the rub-grooves of the honeycomb samples along with extrusion deformation, and it presents most obviously in test 7#. Because of the foil's structure, the cutting debris of honeycomb is usually lamellar and curly. During the rubbing process, some wear debris
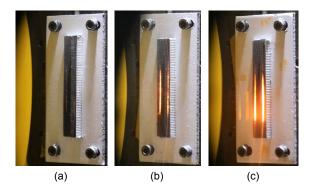

Fig. 14 Friction sparks at the end of different rubbing tests: (a) V_b=150 m/s; (b) V_b=300 m/s; (c) V_b=450 m/s
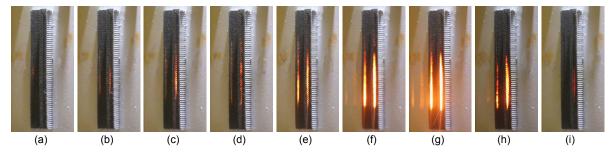

Fig. 13 Video recording of one rubbing process (V_b=450 m/s, V_r=120 μm/s)
(a) t=0 s; (b) t=2 s; (c) t=4 s; (d) t=6 s; (e) t=8 s; (f) t=10 s; (g) t=12 s; (h) t=14 s; (i) t=16 s
Note: for interpretation of the references to color, the reader is referred to the web version of this article

may be transferred to the blade and accumulated at the end of labyrinth tip, leading to the increase of blade tip width.

These first observations suggest that the wear mechanisms of metal honeycomb are cutting, compression deformation, smearing, oxidation, and adhesive transfer. The mechanisms of the turbine blade when rubbing with a honeycomb structure are wear, thermal ablation, and oxidation.

3.2 Analysis of rubbing forces

As the sharp-edged labyrinth blade sweeps through the honeycomb at a high linear velocity, interaction forces will be produced in radial and tangential directions. The radial extrusion force is caused by the incursion movement of the honeycomb specimen, and the tangential scraping force is similar to the usual cut or friction force. Rubbing force is to some extent a critical characterization of damage degree, and this may cause the deformation and damage of the honeycomb material and the wear of blade. A wealth of information can be acquired from interaction forces, such as scraping difficulty and uniformity, which will be used to evaluate the abradable performance of a honeycomb material and to study the high speed rubbing phenomenon between the abradable seal material and the blade material.

The force measuring system of the abradable tester can be described as a mass-spring-damper system, and an attenuation response will be generated when the rubbing force is input, and this can be simplified and represented as a rectangular pulse force (Zhang *et al.*, 2016). The typical radial and tangential forces over time for a single rubbing cycle are shown in Fig. 15. It is found that the radial force has the similar trend to the tangential one, except that the radial force is a little larger. After removing the damping effect, we find that only the amplitude value is useful for the description of rubbing forces in a single rubbing cycle.

Representative radial and tangential forces during the whole rubbing process are illustrated in Fig. 16. Each force curve is composed of four stages: the first is pre-rubbing stage (0–1 s), the second is rubbing stage (1–13.9 s), the third and the fourth are holding stage (13.9–15.9 s) and termination stage (15.9–17 s), respectively. Pre-rubbing stage is the test time before the honeycomb sample contacts with the

blade labyrinth, in which the rubbing forces are stable with almost zero value because of the basic vibration of tester and signal interference. When the labyrinth tip contacts the honeycomb surface, a sudden increase of rubbing force is shown in the radial and tangential directions simultaneously, and because of the small scraping area at the beginning of the rubbing stage, a uniform and stable rubbing action with tiny chips is presented. As shown in Eq. (4), the scraping area gradually increases with rubbing time, and the rubbing forces also gradually become larger and larger until the rubbing time reaches 10 s. Then during 10–13.9 s the influence of the scraping area on the
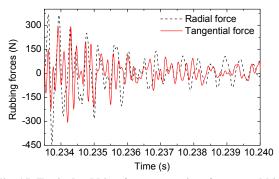

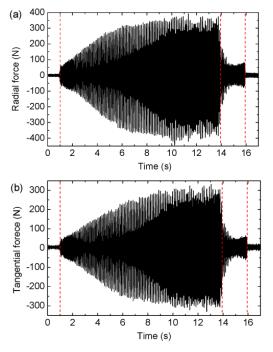**Fig. 15 Typical rubbing forces over time for one rubbing cycle (V_b=300 m/s, V_r=120 µm/s)**

Fig. 16 Radial (a) and tangential (b) forces recorded over the rubbing period (V_b=300 m/s, V_r=120 µm/s)

rubbing forces reduces, and a relatively stable trend with slight fluctuations is shown. The duration of the rubbing stage is about 12.9 s, which is longer than the theoretical time of 8.3 s for a total incursion depth of 1 mm. That is because the initial zero depth is calibrated under static conditions and then elastic extension deformation of the blade and disk with a high rotating speed leads to the contact in advance. During the 2 s of the holding stage, rubbing forces decrease rapidly from 300 N to 70 N, and a very slightly rubbing action still exists although there is no incursion movement. At the end, the honeycomb sample leaves the labyrinth tips rapidly with the forces reducing to small values in the terminal stage, and these are mainly signal interference and the basic vibration of the tester.

Because of the elastic extension deformation of the blade and disk, the actual incursion depth is larger than the theoretical one, and the higher the blade tip speed is, the bigger the difference will be. Therefore, to evaluate the force with different blade tip speeds, the force data during the incursion depth of 0–1 mm are separated out, and the maximum value of the rubbing force is defined as an evaluation parameter for the whole rubbing process. Table 2 and Fig. 17 show the maximum rubbing force data of nine tests. It is found that with a low blade tip speed, such as 150 m/s, the radial force is usually higher than the tangential one, resulting in a rubbing coefficient smaller than 1.0. Under this condition, the radial extrusion mechanism is much more dominant than cutting, smearing, and other mechanisms. However, with the increase of blade tip speed, the cutting action gradually becomes the predominant fail mode with smearing and oxidation for honeycomb material based on much more impact energy. The result is that the tangential force becomes larger than the radial one, which means a rubbing coefficient greater than 1.0. On the other side, a similar tendency with different blade tip speeds and incursion rates is shown for the tangential and radial forces. The maximum rubbing force of the test with a blade tip speed of 300 m/s is larger than those of 150 m/s and 450 m/s at the same incursion rate, no matter whether it is in the tangential or radial direction. Under the condition of 300 m/s, the rubbing force presents a steady growth with the increase of incursion rate. At blade tip speeds of 150 m/s and 450 m/s, however, the trend of first de-

creasing and then increasing is shown. The maximum forces in radial and tangential directions are 716 N and 871 N, respectively under the condition of 300 m/s blade tip speed and 360 μm/s incursion rate, and neither would cause damage to the rotating blade labyrinth.

Table 2 Recorded data of rubbing force and acceleration

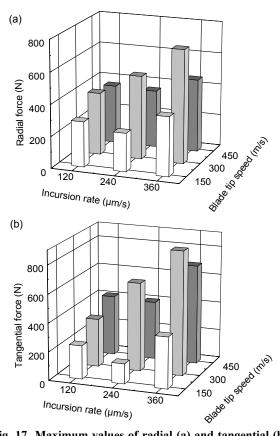| Test No.	Max. radial force, $F_{r,max}$ (N)	Max. tangential force, $F_{t,max}$ (N)	Rubbing coefficient, μ_f	Acceleration, A_r ($\times g$)
1#	284.1	233.5	0.82	106.7
2#	241.5	141.0	0.58	77.5
3#	372.5	360.0	0.97	124.5
4#	391.3	331.0	0.85	151.2
5#	525.2	620.5	1.18	221.0
6#	715.7	870.6	1.22	278.5
7#	368.7	419.4	1.14	327.8
8#	361.5	407.8	1.13	207.6
9#	459.3	695.3	1.51	341.0

Fig. 17 Maximum values of radial (a) and tangential (b) forces for nine tests

3.3 Analysis of rubbing accelerations

The rubbing process between the blade tip and honeycomb sample is a high-speed impact phenomenon, so the acceleration response of the sample is a critical parameter used for rubbing analysis. In the local rubbing process, an obvious feature of periodical impulsion is extracted. There is a transient acceleration with large amplitude in the instant of rubbing, followed by gradually attenuated signals. The acceleration curve is illustrated in Fig. 18. Its changing trend during the whole rubbing process is similar to the rubbing force, and the four stages can be separated out from the curve. In our rubbing tests, the maximum values of impact acceleration during the incursion depth of 0–1 mm are the emphasis of the rubbing tests, and have been listed in Table 2. The data show that recorded acceleration is changing with blade tip speed and incursion rate. A significant increase of acceleration is recorded when the values of blade tip speed increase. However, it shows a different variation trend with the increase of incursion rate at different blade tip speeds. As shown in Fig.19, at blade tip speeds of 150 m/s and 450 m/s, the acceleration first decreases and then increases with the increase of incursion rate, but it only increases at the blade tip of 300 m/s. Despite all this, the acceleration at an incursion rate of 360 μm/s is larger than that at 120 μm/s. This trend is consistent with the finding on the rubbing forces. The difference is that the accelerations of tests 7# and 9# at the blade tip speed of 450 m/s are larger than tests 4#, 5#, and 6# at 300 m/s. The highest acceleration value for this set of tests is 341g under the highest blade tip speed of 450 m/s and the highest incursion rate of 360 μm/s.
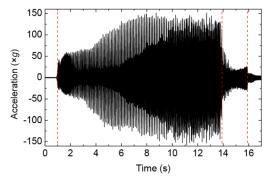

Fig. 18 Variation curve of acceleration (V_b=300 m/s, V_r=120 μm/s)
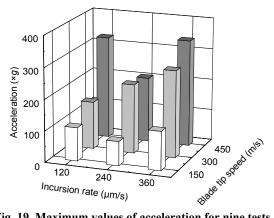

Fig. 19 Maximum values of acceleration for nine tests

4 Conclusions

The coupling of a metal honeycomb structure and stepped labyrinth has been widely used for decades to improve the efficiency of turbo-engines. To get a better understanding of their high-speed rubbing behavior, nine rubbing experiments were carried out between a Hastelloy-X honeycomb and a double labyrinth blade of GH4169 with blade tip speeds of 150–450 m/s and incursion rates of 120–360 μm/s using a high-speed abradable test rig with the maximum blade tip speed of 520 m/s. Visual rubbing observations, maximum rubbing forces, and impact acceleration analysis under different test parameters provide a lot of information for the first assessment.

1. Compression deformation occurs on the honeycomb material during the rubbing process with a labyrinth blade except for the cutting mechanism, and it is mainly affected by the parameter of incursion rate.

2. An obvious friction spark has been observed from video recording, which is useful in explaining thermal ablation and oxidation mechanisms occurring on the turbine blade. Frictional heat will increase and congregate with expansion of the scraping area between the labyrinth tip and honeycomb sample, and it is much more obvious with a higher blade tip speed. Moreover, the accumulated friction heat can cause the smearing of the metal honeycomb and adhesive transfer of honeycomb material to the labyrinth tips.

3. Each rubbing force curve can be separated into four stages: pre-rubbing, rubbing, holding, and termination. The maximum value of the rubbing force

which is affected by blade tip speed and incursion rate can be used as an effective description of the degree of damage during the rubbing process. Under the condition of 300 m/s, the rubbing force presents a steady growth with increase of incursion rate. Under the condition of 150 m/s and 450 m/s, however, a trend of first decreasing and then increasing is shown. With a blade tip speed of 300 m/s and incursion rate of 360 μm/s, radial and tangential forces show their maximum values of 716 N and 871 N, respectively, and neither of them could cause damage to the rotating rotor.

4. Under blade tip speeds of 150 m/s and 450 m/s, the acceleration first decreases and then increases with the increase of incursion rate, but only increases when the blade tip speed is 300 m/s. The peak value of acceleration presents 341*g* in the test with the highest blade tip speed of 450 m/s and the highest incursion rate of 360 μm/s.

References

Bardi, U., Giolli, C., Scrivani, A., *et al*., 2008. Development and investigation on new composite and ceramic coatings as possible abradable seals. *Journal of Thermal Spray Technology*, **17**(5-6):805-811.
http://dx.doi.org/10.1007/s11666-008-9246-5

Bill, R.C., Shiembob, L.T., 1977. Friction and wear of sintered fiber-metal abradable seal materials. *Journal of Lubrication Technology*, **99**(4):421-427.
http://dx.doi.org/10.1115/1.3453236

Bill, R.C., Shiembob, L.T., 1981. Some considerations of the performance of two honeycomb gas path seal material systems. *Lubrication Engineering*, **37**(4):209-217.

Bounazef, M., Guessasma, S., Saadi, B.A., 2004. The wear, deterioration and transformation phenomena of abradable coating BN-SiAl-bounding organic element, caused by the friction between the blades and the turbine casing. *Materials Letters*, **58**(27-28):3375-3380.
http://dx.doi.org/10.1016/j.matlet.2004.02.049

Chen, L.S., Wang, Y.L., Lu, J.H., *et al*., 2008. Development of study and application of aeroengine sealing technology. *Aeronautical Manufacturing Technology*, (8):82-95 (in Chinese).
http://dx.doi.org/10.16080/j.issn1671-833x.2008.08.014

Chupp, R., Ghasripoor, F., Moore, G., 2002. Applying abradable seals to industrial gas turbines. 38th AIAA/ASME/SAE/ASEE Joint Propulsion Conference & Exhibit, Indianapolis, USA. AIAA, Virginia, USA, p.3795.
http://dx.doi.org/10.2514/6.2002-3795

Chupp, R.E., Lau, Y.C., Ghaspripoor, F., *et al*., 2004. Development of higher temperature abradable seals for gas turbine applications. ASME Turbo Expo 2004: Power for Land, Sea, and Air, Vienna, Austria. ASME, New York, USA, p.221-229.
http://dx.doi.org/10.1115/GT2004-53029

Collins, D., Teixeira, J., Crudgington, P., 2008. The degradation of abradable honeycomb labyrinth seal performance due to wear. *Sealing Technology*, **2008**(8):82-84.
http://dx.doi.org/10.1016/S1350-4789(08)70451-3

Dadouche, A., Conlon, M.J., Dmochowski, W., 2008. Experimental evaluation of abradable seal performance at high temperature. ASME Turbo Expo 2008: Power for Land, Sea, and Air, Berlin, Germany. ASME, New York, USA, p.143-150.
http://dx.doi.org/10.1115/GT2008-51228

Dalzell, W.J., Sanders, S.A., Crawford, G.L., *et al*., 2002. Abradable seal with improved properties. *Sealing Technology*, **2002**(8):14-15.
http://dx.doi.org/10.1016/S1350-4789(02)08036-4

DeMasi-Marcin, J.T., Gupta, D.K., 1994. Protective coatings in the gas turbine engine. *Surface and Coatings Technology*, **68-69**:1-9.
http://dx.doi.org/10.1016/0257-8972(94)90129-5

Delebarre, C., Wagner, V., Paris, J.Y., *et al*., 2014. An experimental study of the high speed interaction between a labyrinth seal and an abradable coating in a turbo-engine application. *Wear*, **316**(1-2):109-118.
http://dx.doi.org/10.1016/j.wear.2014.04.023

Dorfman, M., Erning, U., Mallon, J., 2002. Gas turbines use 'abradable' coatings for clearance-control seal. *Sealing Technology*, **2002**(1):7-8.
http://dx.doi.org/10.1016/S1350-4789(02)80002-2

Dowson, P., Walker, M.S., Watson, A.P., 2004. Development of abradable and rub-tolerant seal materials for application in centrifugal compressors and steam turbines. *Sealing Technology*, **2004**(12):5-10.
http://dx.doi.org/10.1016/S1350-4789(04)00451-9

Draskovich, B.S., Frani, N.E., Joseph, S.S., *et al*., 1998. Abrasive Tip/Abradable Shroud System and Method for Gas Turbine Compressor Clearance Control. US Patent 5704759.

Fois, N., Stringer, J., Marshall, M.B., 2013. Adhesive transfer in aero-engine abradable linings contact. *Wear*, **304**(1-2):202-210.
http://dx.doi.org/10.1016/j.wear.2013.04.033

Fu, L., Feng, Z.P., Li, G.J., *et al*., 2015. Experimental validation of an integrated optimization design of a radial turbine for micro gas turbines. *Journal of Zhejiang University-SCIENCE A (Applied Physics & Engineering)*, **16**(3):241-249.
http://dx.doi.org/10.1631/jzus.A1400073

Ghasripoor, F., Dorfman, M., Schmid, R., 1997. Abradables improve gas turbine efficiency. *Materials World*, **5**(6):328-330.

He, K., Li, J., Yan, X., *et al*., 2012. Investigation of the conjugate heat transfer and windage effect in stepped labyrinth seals. *International Journal of Heat and Mass Transfer*, **55**(17-18):4536-4547.
http://dx.doi.org/10.1016/j.ijheatmasstransfer.2012.03.045

Ma, X., Matthews, A., 2007. Investigation of abradable seal coating performance using scratch testing. *Surface and Coatings Technology*, **202**(4-7):1214-1220.
http://dx.doi.org/10.1016/j.surfcoat.2007.07.076

Ma, X.F., Duan, Z., Shi, H.J., *et al*., 2010. Fatigue and fracture behavior of nickel-based superalloy Inconel 718 up to the very high cycle regime. *Journal of Zhejiang University-SCIENCE A (Applied Physics & Engineering)*, **11**(10):727-737.
http://dx.doi.org/10.1631/jzus.A1000171

Miao, R.H., 2008. Application of metal cellular gas-tight seal in steam turbine. *Taiyuan Science and Technology*, (2):68-72 (in Chinese).
http://dx.doi.org/10.3969/j.issn. 1674-9146.2008.02.030

Padova, C., Barton, J., Dunn, M.G., *et al*., 2006. Experimental results from controlled blade tip/shroud rubs at engine speed. *Journal of Turbomachinery*, **129**(4):713-723.
http://dx.doi.org/10.1115/1.2720869

Potter, D.J., Chai, Y.W., Tatlock, G.J., 2009. Improvements in honeycomb abradable seals. *Materials at High Temperatures*, **26**(2):127-135.
http://dx.doi.org/10.3184/096034009X464302

Pychynski, T., Höefler, C., Bauer, H.J., 2015. Experimental study on the friction contact between a labyrinth seal fin and a honeycomb stator. *Journal of Engineering for Gas Turbines and Power*, **138**(6):062501.
http://dx.doi.org/10.1115/1.4031791

Rathmann, U., Olmes, S., Simeon, A., 2007. Sealing technology: rub test rig for abrasive/abradable systems. ASME Turbo Expo 2007: Power for Land, Sea, and Air, Montreal, Canada. ASME, New York, USA, p.223-228.
http://dx.doi.org/10.1115/GT2007-27724

Schmid, R.K., Ghasripoor, F., Dorfman, M., *et al*., 2000. An overview of compressor abradable thermal spray. Proceedings of Surface Engineering Interaction Thermal Spray Conference ITSC, Montreal, Canada, p.1087-1093.

Shen, H., Zheng, T.H., Chen, Y.J., 2011. Improvement of aero-engine sealing technology. *Gas Turbine Experimental and Research*, **24**(4):51-55 (in Chinese).
http://dx.doi.org/10.3969/j.issn.1672-2620.2011.04.014

Shen, M.X., Zheng, J.P., Meng, X.K., *et al*., 2015. Influence of Al$_2$O$_3$ particles on the friction and wear behaviors of nitrile rubber against 316L stainless steel. *Journal of Zhejiang University-SCIENCE A (Applied Physics & Engineering)*, **16**(2):151-160.
http://dx.doi.org/10.1631/jzus.A1400217

Sporer, D.R., Shiembob, L.T., Sporer, D.R., *et al*., 2004. Alloy selection for honeycomb gas path seal systems. ASME Turbo Expo 2004: Power for Land, Sea, and Air, Vienna, Austria. ASME, New York, USA, p.763-774.
http://dx.doi.org/10.1115/GT2004-53115

Stringer, J., Marshall, M.B., 2012. High speed wear testing of an abradable coating. *Wear*, **294-295**(31):257-263.
http://dx.doi.org/10.1016/j.wear.2012.07.009

Vakili, A.D., Meganathan, A.J., Michaud, M., *et al*., 2005. An experimental and numerical study of labyrinth seal flow. ASME Turbo Expo 2005: Power for Land, Sea, and Air, Reno, Nevada, USA. ASME, New York, USA, p.1121-1128.
http://dx.doi.org/10.1115/GT2005-68224

Wei, L.J., Li, C.Q., Gao, L., *et al*., 2005. Application and development of steam turbine sealing technology. *Journal of Engineering for Thermal Energy and Power*, **20**(5):455-458 (in Chinese).
http://dx.doi.org/10.3969/j.issn.1001-2060.2005.05.002

Wiebe, D.J., 1994. Abradeable Labyrinth Stator Seal. US Patent 5314304.

Wu, J.H., 2011. Compound cellular steam seal and its application on turbine shaft seal. *Journal of Shenyang Institute of Engineering (Natural Science)*, **7**(1):24-28 (in Chinese).
http://dx.doi.org/10.3969/j.issn.1673-1603.2011.01.007

Zhang, N., Shen, J., Xuan, H.J., *et al*., 2016. Evaluation of an AlSi-polyester abradable seal coating performance using high-temperature and high-velocity abrasion tests. *Proceedings of the Institution of Mechanical Engineers, Part J: Journal of Engineering Tribology*, **230**(7):842-851.
http://dx.doi.org/10.1177/1350650115619150

Zhang, X.L., Yao, B., Feng, W., *et al*., 2015. Modeling of a virtual grinding wheel based on random distribution of multi-grains and simulation of machine-process interaction. *Journal of Zhejiang University-SCIENCE A (Applied Physics & Engineering)*, **16**(11):874-884.
http://dx.doi.org/10.1631/jzus.A1400316

中文概要

题　目：涡轮发动机中篦齿-蜂窝封严结构的高速碰磨行为研究

目　的：航空涡轮发动机中篦齿-蜂窝封严结构能有效降低转动部件之间的气路间隙，提高发动机效率。在高温高速可磨耗试验机上进行模拟试验，研究篦齿叶尖与金属蜂窝之间的高速碰磨行为，分析篦齿叶片和金属蜂窝的磨耗机理，验证金属蜂窝的可磨耗性能，为蜂窝封严在航空发动机中的应用提供参考。

创新点：1. 成功研制了模拟封严材料高速碰磨行为的可磨耗试验机，最高叶尖线速度可达 520 m/s；2. 进行了不同试验条件下的高速碰磨试验，验证了蜂窝材料的可磨耗性能；3. 通过高速碰磨试验，掌握篦齿叶片和金属蜂窝的磨耗机理；4. 获得了高速碰摩力和冲击加速度数据，对应用具有指导作用。

方　法： 1. 研制高速可磨耗试验机；径向进给系统驱动封严试样主动与高速旋转的模拟叶片接触并发生高速碰磨作用；试验机可模拟的最高叶尖线速度为 520 m/s，进给速率为 5~1000 μm/s。2. 在可磨耗试验机上进行不同叶尖线速度和进给速率条件下的高速碰磨试验，通过对试验现象以及试验后金属蜂窝和篦齿叶片的磨损形貌进行分析，了解高速碰磨过程中的磨损机理。3. 通过三向测力传感器对试验中的高速碰磨力进行测量，分析碰磨力的变化规律。4. 通过加速度传感器测量瞬时冲击响应，了解冲击作用的大小。

结　论： 1. 高速碰磨时，金属蜂窝会发生切削和挤压变形，进给速率对挤压变形具有重要影响。2. 高速碰磨时篦齿与蜂窝的接触区域会产生摩擦火花，导致篦齿叶尖发生烧蚀和氧化，摩擦热的聚集会导致蜂窝材料在被切削时发生涂抹，同时伴随有蜂窝材料向篦齿叶尖的转移。3. 随着碰磨时间的延长，摩擦热逐渐增多，且在高叶尖线速度条件下更加明显。4. 测试到的碰摩力曲线可以分为四个典型阶段：碰磨前、碰磨中、停留和退出；试验测试到的最大径向和切向碰摩力分别为 716 N 和 871 N，不会对转子部件造成损坏。5. 在最大叶尖线速度和最大进给速率参数下测得的冲击加速度最大，约为 341g。

关键词： 篦齿-蜂窝封严；航空发动机带冠涡轮叶片；可磨耗性；碰磨机理；碰磨作用